



HAL
open science

Modeling of heat flow and effective thermal conductivity of fractured media: Analytical and numerical methods

Sy Tuan Nguyen, Manh Huyen Vu, Minh Ngoc Vu, Anh Minh A.M. Tang

► To cite this version:

Sy Tuan Nguyen, Manh Huyen Vu, Minh Ngoc Vu, Anh Minh A.M. Tang. Modeling of heat flow and effective thermal conductivity of fractured media: Analytical and numerical methods. *Journal of Applied Geophysics*, 2017, 140, pp.117-122. 10.1016/j.jappgeo.2017.03.018 . hal-01515979

HAL Id: hal-01515979

<https://enpc.hal.science/hal-01515979>

Submitted on 16 May 2019

HAL is a multi-disciplinary open access archive for the deposit and dissemination of scientific research documents, whether they are published or not. The documents may come from teaching and research institutions in France or abroad, or from public or private research centers.

L'archive ouverte pluridisciplinaire **HAL**, est destinée au dépôt et à la diffusion de documents scientifiques de niveau recherche, publiés ou non, émanant des établissements d'enseignement et de recherche français ou étrangers, des laboratoires publics ou privés.

1 **Modeling of heat flow and effective thermal conductivity of fractured media:**
2 **analytical and numerical methods**

3 *S.T. Nguyen^(a,b,*), M.-H. Vu^(b), M.N. Vu^(b) and A.M. Tang^(c)*

4 *(a) Euro-Engineering, Pau, France*

5 *(b) R&D Center, Duy Tan University, Da Nang, Viet Nam*

6 *(c) Université Paris-Est, Laboratoire Navier (ENPC-IFSTTAR-CNRS) 77455 Marne la*
7 *Vallée, France*

8 *(*) Corresponding author: stuan.nguyen@gmail.com*

9 **Abstract**

10 The present work aims at modeling the thermal conductivity of fractured materials using
11 homogenization-based analytical and pattern-based numerical methods. These materials are
12 considered as a network of cracks distributed inside a solid matrix. Heat flow through such
13 media is perturbed by the crack system. The problem of heat flow across a single crack is
14 firstly investigated. The classical Eshelby's solution, extended for the calculation of the
15 conductivity of a mixture of an ellipsoidal inclusion in an infinite homogeneous matrix, gives
16 an analytical solution of temperature discontinuity across a non-conducting penny-shape
17 crack. This solution is then validated by the numerical simulation based on the finite
18 elements method. The numerical simulation allows analyzing the effect of crack conductivity.
19 The problem of a single crack is then extended to media containing multiple cracks.
20 Analytical estimations for effective thermal conductivity, that take into account the interaction
21 between cracks and their spatial distribution, are developed for the case of non-conducting
22 cracks. Pattern-based numerical method is then employed for both cases non-conducting
23 and conducting cracks. In the case of non-conducting cracks, numerical and analytical
24 methods, both account for the spatial distribution of the cracks, fit perfectly. In the case of
25 conducting cracks, the numerical analyzing of crack conductivity effect shows that highly
26 conducting cracks weakly affect heat flow, and the effective thermal conductivity of fractured
27 media.

28 **Keywords:** morphologically representative pattern; thermal conductivity; homogenization;
29 fractured rock

30 **1. Introduction**

31 Thermal conductivity is an important geophysical property of rocks and largely investigated in
32 geo-sciences such as, nuclear waste disposal, geothermal production, CO₂ storage,
33 hydrocarbon formation processes, etc (Tang and Cui, 2009; Tang et al., 2008; Cui et al,
34 2011). This parameter is generally affected by natural cracks distributed in the geomaterials.
35 The homogenization-based analytical approach has been confirmed to be a powerful tool to
36 estimate effective properties of heterogeneous materials (Eshelby, 1957; Mori and Tanaka,
37 1973; Giraud et al., 2007; Zimmerman, 1989). The macroscopic mechanical properties is
38 affected by the properties of each phase in the mixture, the shape and the orientation of the
39 particles as well as the stress acting on the considered materials. Nguyen and colleagues
40 successfully employed this technique for the simulation of effective viscoelastic properties of
41 fractured media (Nguyen et al., 2011, Nguyen, 2014a; Nguyen et al., 2015c) and effective
42 elastic properties and electrical conductivity of sandstone (Nguyen, 2014b, Nguyen et al,
43 2015a,b).

44 Besides, the numerical approach based on the pattern-based method (PBM) is also used to
45 simulate overall properties of heterogeneous materials (Bornert, 1996; Stolz and Zaoui,
46 1991). This approach is more powerful than the classical numerical finite element method
47 (FEM) that simulates the whole representative elementary volume (REV) of the medium, in
48 term of calculation time. Actually, the PBM considers a morphologically representative
49 pattern (MRP) of the medium instead of the REV. For the case of fractured media, MRP
50 contains only one crack whereas REV contains a whole system of micro-cracks (Pouya et
51 al., 2013; Camacho and Ortiz, 1996). However, by managing the boundary condition and the
52 shape of the MRP, the pattern-based method allows accounting for the interaction between
53 cracks and their spatial distribution (Nguyen and Dormieux, 2014).

54 This paper focuses on the thermal conductivity of fractured materials based on
55 homogenization-based analytical method and PBM. The problem of heat flow through a
56 medium containing a single crack is firstly considered. The classical Eshelby's theory,
57 extended for the conductivity of a mixture of an ellipsoidal inclusion in an infinite
58 homogeneous matrix, gives an analytical solution of temperature discontinuity across a non-
59 conducting penny-shape crack. This analytical solution is then compared with the numerical
60 simulation based on PBM. The effect of crack conductivity is also analyzed with the help of
61 the numerical simulation. Secondly, the problem of single crack is extended to a medium
62 containing multiple cracks. Analytical estimations of effective thermal conductivity for the
63 case of non-conducting cracks, that accounts the interaction between the cracks and their
64 spatial distribution, are developed. PBM is then employed for both cases, non-conducting
65 and conducting cracks.

66 **Notations**

- 67 ▪ \mathbf{A} is the second order temperature field localization tensor
- 68 ▪ $\mathbf{1}$ is the second order unit tensor
- 69 ▪ $[T]$ is the temperature jump across a crack
- 70 ▪ $[t]$ is the dimensionless temperature jump across a crack
- 71 ▪ ∇T is the temperature gradient
- 72 ▪ \underline{z} is the position vector of a point
- 73 ▪ f is the volume fraction
- 74 ▪ C is the conductivity
- 75 ▪ Q is the anisotropic parameters of the inclusion
- 76 ▪ X and X_d are the aspect ratio of the cracks and of the spatial distribution of the cracks
77 respectively

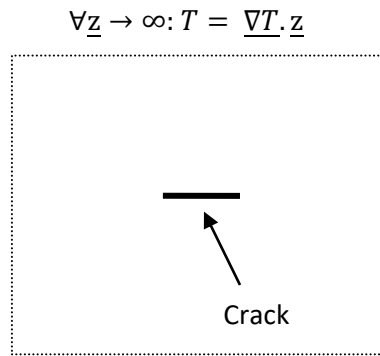
78 The exponents and index

- 79 ▪ s is for the solid phase
- 80 ▪ c is for crack

- 81 ▪ T is for transversal component of the transversely isotropic tensors
- 82 ▪ N is for normal component of the transversely isotropic tensors
- 83 ▪ mt is for Mori-Tanaka scheme
- 84 ▪ cw is for Castañeda-Willis scheme

85 **2. Heat flow across a single crack**

86 One considers a basic problem of a single crack in a homogenous medium under a far-field
 87 homogenous temperature gradient condition: $\forall \underline{z} \rightarrow \infty: T = \underline{\nabla T} \cdot \underline{z}$ (see Fig. 1). Heat flow is
 88 locally perturbed around the crack due to the contrast between the conductivity of the crack
 89 and that of the surrounding solid matrix. Temperature is discontinued across the crack.



90

91 *Figure1: Single crack in homogenous medium under far-field homogeneous temperature*
 92 *gradient boundary condition.*

93 Note that for penny-shape crack, an extension of Eshelby's theory (Eshelby, 1957) for the
 94 problem of heat flow yields a temperature field localization tensor A that is determined by
 95 (Giraud, 2007; Nguyen, 2014):

$$A = \frac{C_s}{(1-Q)C_s + QC_c} (\mathbf{1} - \underline{e}_3 \otimes \underline{e}_3) + \frac{C_s}{2QC_s + (1-2Q)C_c} \underline{e}_3 \otimes \underline{e}_3 \quad (1)$$

96 where C_s (resp. C_c) is the conductivity of the solid matrix (resp. the conductivity of the crack),
 97 \underline{e}_3 the unit normal to the crack plan, and Q the geometry factor defined by:

$$Q = \frac{1}{2} - \frac{\sqrt{1-X^2} - X \arctan\left(\frac{\sqrt{1-X^2}}{X}\right)}{2(1-X^2)^{3/2}} \quad (2)$$

98 with X is the aspect ratio of the crack (ratio between the width and the diameter of the crack,
 99 see also Dormieux, 2006). Thus, for penny-shape crack we have: $X \rightarrow 0$ and

$$Q \approx \frac{\pi}{4} X \quad (3)$$

100 Introducing eq. (3) into eq. (1) yields:

$$\mathbf{A} = \frac{C_s}{\left(1 - \frac{\pi}{4} X\right) C_s + \frac{\pi}{4} X C_c} (\mathbf{1} - \underline{e}_3 \otimes \underline{e}_3) + \frac{C_s}{\frac{\pi}{2} X C_s + \left(1 - \frac{\pi}{2} X\right) C_c} \underline{e}_3 \otimes \underline{e}_3 \quad (4)$$

101 The local temperature gradient inside the crack, $\underline{\nabla} T_c$ is homogeneous and is linearly related
 102 to the far-field temperature gradient (Fig. 1) as:

$$\underline{\nabla} T_c = \mathbf{A} \cdot \underline{\nabla} T \quad (5)$$

103 Its component normal to the crack plan is expressed as:

$$\nabla T_{c,3} = \frac{C_s}{\frac{\pi}{2} X C_s + \left(1 - \frac{\pi}{2} X\right) C_c} \nabla T_3 \quad (6)$$

104 According to this solution, the temperature jump across the crack $[T]$ is calculated as:

$$[T] = \nabla T_{c,3} d = \left(\frac{C_s}{\frac{\pi}{2} X C_s + \left(1 - \frac{\pi}{2} X\right) C_c} \nabla T_3 \right) d \quad (7)$$

105 where d is the distance between two crack's lips at the considering point. Suppose that the
 106 crack has a spheroidal shape, d is calculated by:

$$d = 2X\ell \sqrt{1 - \left(\frac{\rho}{\ell}\right)^2} \quad (8)$$

107 where ℓ and ρ are the radius of the crack and the distance to the crack's center, respectively.

108 The combination of (7) and (8) yields:

$$[T] = \left(\frac{C_s}{\frac{\pi}{2}XC_s + \left(1 - \frac{\pi}{2}X\right)C_c} \nabla T_3 \right) 2X\ell \sqrt{1 - \left(\frac{\rho}{\ell}\right)^2} \quad (9)$$

109 It is convenient to introduce also the following dimensionless temperature discontinuity:

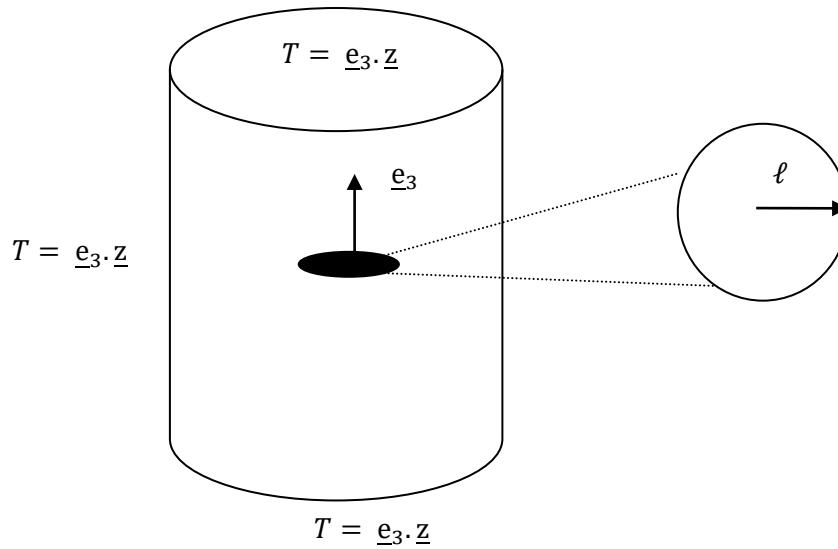
$$[t] = \frac{[T]}{\nabla T_3} \frac{1}{\ell} = \left(\frac{2XC_s}{\frac{\pi}{2}XC_s + \left(1 - \frac{\pi}{2}X\right)C_c} \right) \sqrt{1 - \left(\frac{\rho}{\ell}\right)^2} \quad (10)$$

110 For the case of conducting crack, i.e. $C_c > 0$, the limit $X \rightarrow 0$ (penny-shape crack) yields $[t] \rightarrow$
 111 0. More precisely, there is no temperature jump across a penny-shape conducting crack. For
 112 the case of non-conducting penny-shape crack ($C_c = 0$), equation (10) is simplified (see also
 113 Sevostianov, 2006; Vu et al., 2015) as:

$$[t] = \frac{4}{\pi} \sqrt{1 - \left(\frac{\rho}{\ell}\right)^2} \quad (11)$$

114 The maximum value of $[t] = 4/\pi$ is found at the center of the crack ($\rho = 0$). The analytical
 115 solution (11) could be considered as a reference to compare with the numerical simulation.

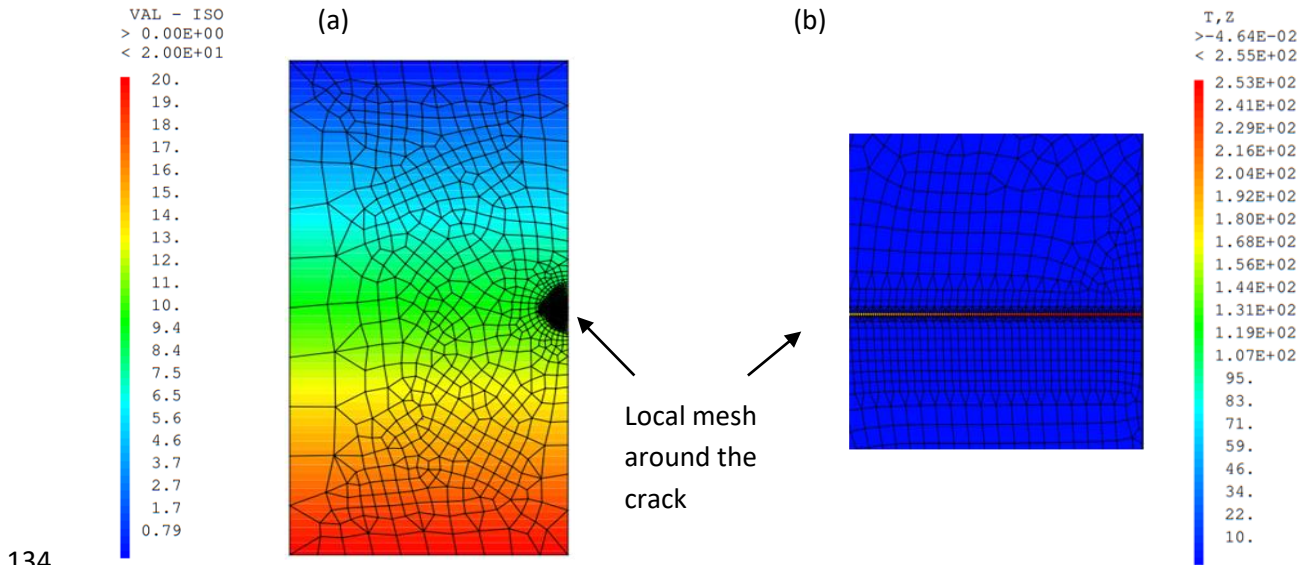
116 Considering the FEM approach for the simulation of this basic problem of heat flow across a
 117 single crack, a vertical cylinder containing a horizontal penny-shape crack is analyzed (Fig.
 118 2). Unit vertical temperature gradient is applied on the boundary of the cylinder: $T = \underline{e}_3 \cdot \underline{z}$.
 119 The dimension of the cylinder is chosen large enough to ensure the far-field boundary
 120 condition. The calculation is performed in axis symmetric model thank to the symmetry of the
 121 problem.



122

123 *Figure 2: Numerical simulation of heat flow across a single crack: geometry and boundary*
 124 *conditions.*

125 In this model, the crack is defined by a thin horizontal domain with a given conductivity. Zero
 126 conductivity is chosen for the crack's domain when modeling a non-conducting crack. The
 127 thickness of the crack domain is chosen small enough to ensure the convergence of the
 128 results. It is verified that, a ratio between the thickness and the radius of the crack smaller
 129 than 0.005 is enough. The mesh is refined around the crack, therefore a too small crack's
 130 thickness will unnecessarily raise the calculation time. The simulation is carried out by using
 131 FEM codes Cast3M (Bentejac and Hourdequin, 2005). Fig. 3 displays the mesh (in axis
 132 symmetric model), the temperature distribution in the whole domain (left side) and the local
 133 vertical temperature gradient across the crack (right side).

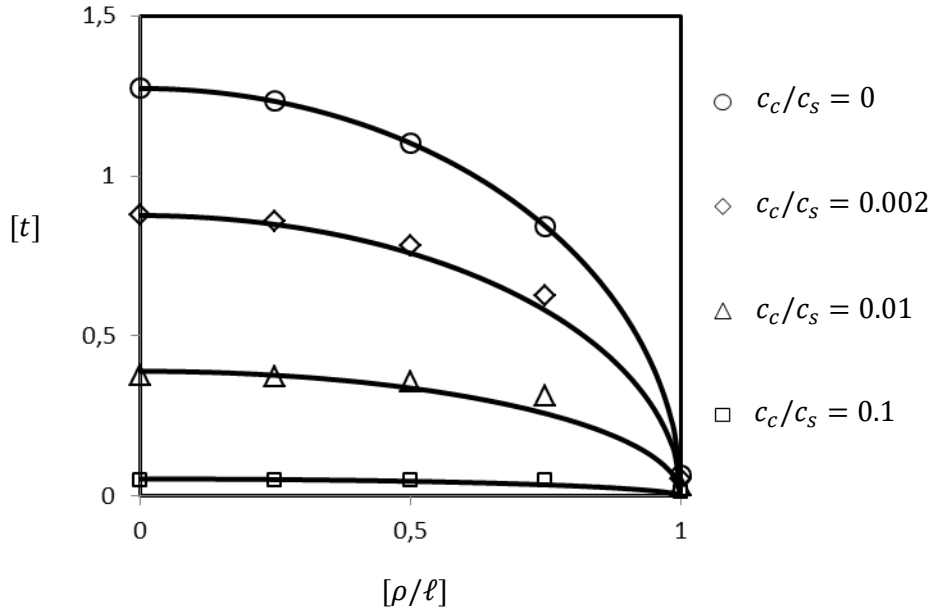


136 *Figure 3: Numerical simulation of heat flow across a single crack: (a) temperature*
 137 *distribution; (b) Local temperature gradient across the crack.*

138 In the particular case of non-conducting crack, the numerical simulation of the temperature
 139 jump across the crack is compared with the analytical solution given by the eq. (11). Fig. 4
 140 shows the dimensionless temperature discontinuity along the crack radius. A perfect fit
 141 between the numerical and the analytical approaches can be observed.

142 Note that the solution given by eq. (11) is for non-conducting crack such as open and dry
 143 crack. However fluid saturated or partially saturated crack and closed crack are conducting.
 144 Fig. 4 shows also the effect of the relative conductivity of the crack and of the surrounding
 145 solid matrix on the temperature jump across the crack. For $C_c/C_s \approx 0.1$, the temperature jump
 146 is negligible. For the case of water saturated cracks in rocks (based on data given by Clauser
 147 and Huenges, 1995): $C_c/C_s = C_{water}/C_s \approx 0.1 \div 0.3$. For this case, cracks do not affect the
 148 heat flow across the crack in its normal direction.

149 The basic solutions developed for heat flow across a single crack will be employed and
 150 generalized in the following to simulate the effective conductivity of a domain containing
 151 multiple cracks.



152

153 *Figure 4: Temperature jump across the crack: numerical simulation (the points) and*
 154 *analytical result using eq. (10) (continuous line).*

155 3. Effective thermal conductivity of cracked media

156 This section is dedicated to deriving the effective conductivity of media containing multiple
 157 cracks. First, the analytical homogenization-based approaches for the case of non-
 158 conducting penny-shape cracks is summarized. Second, a pattern-based numerical
 159 approach for both non-conducting and conducting cracks is developed. For non-conducting
 160 penny-shape crack, the numerical simulation is compared and constrained with the analytical
 161 estimations. The effect of crack conductivity on the effective conductivity of the whole
 162 fractured domain is considered at the end of this section.

163 3.1. Homogenization-based approaches

164 The analytical solution (11) of temperature discontinuity across a single crack is a key issue
 165 for the estimation of effective thermal conductivity for fractured media. For the case of
 166 horizontal parallel cracks in an isotropic homogeneous matrix, the effective conductivity of
 167 the medium is transversely isotropic and has on two components: conductivity in the normal

168 direction to the plan of the cracks (\underline{e}_3) and transversal conductivity. The classical Mori-
 169 Tanaka's approach, accounting the fracture interaction, gives (Mori and Tanaka, 1973;
 170 Giraud et al., 2007; Nguyen, 2014):

$$\begin{aligned} C_{mt}^N &= C_s + f_c(C_c - C_s)a^N((1 - f_c) + f_c a^N)^{-1} \\ C_{mt}^T &= C_s + f_c(C_c - C_s)a^T((1 - f_c) + f_c a^T)^{-1} \end{aligned} \quad (12)$$

171 where C_{mt}^N and C_{mt}^T are the normal and transversal conductivity respectively, a^N and a^T the
 172 two corresponding components of the localization tensor defined by eq. (4)

$$a^N = \frac{C_s}{\frac{\pi}{2}XC_s + \left(1 - \frac{\pi}{2}X\right)C_c}; \quad a^T = \frac{C_s}{\left(1 - \frac{\pi}{4}X\right)C_s + \frac{\pi}{4}XC_c} \quad (13)$$

173 The volumetric fraction of the crack is defined by

$$f_c = \frac{4\pi}{3}N\delta\ell^2 = \frac{4\pi}{3}\epsilon X \quad (14)$$

174 where N is the number of cracks in a unit volume of the medium, $\delta = X\ell$ is haft of the crack's
 175 width, $\epsilon = N\ell^3$ is the crack density parameter (see also Budiansky and O'connell, 1976).

176 As discussed in previous section, there is no temperature jump across a penny-shape
 177 conducting crack, i.e. the penny-shape conducting cracks do not affect the effective
 178 conductivity of the medium. Considering now the case of non-conducting penny-shape
 179 cracks $C_c = 0$ and then substituting (13), (14) into (12) yields:

$$C_{mt}^N = C_s \left(1 + \frac{8}{3}\epsilon\right)^{-1}; \quad C_{mt}^T = C_s \quad (15)$$

180 For the case of random orientation distribution of the crack, the conductivity of the whole
 181 domain is isotropic:

$$C_{mt} = \frac{C_{mt}^N + 2C_{mt}^T}{3} = \frac{C_s}{3} \left(2 + \left(1 + \frac{8}{3}\epsilon\right)^{-1}\right) \quad (16)$$

182 The effective conductivity of fractured media can be now estimated for both parallel and
 183 random orientation distribution of cracks, by employing (15) and (16). These results account

184 for the interaction between the cracks but they are limited to the case of non-conducting
 185 cracks. More importantly, these solutions do not account for the spatial distribution of the
 186 cracks (see Castañeda and Willis, 1995; Bornert et al., 1996).

187 To take into consideration the spatial distribution of the cracks, the results obtained by
 188 Gruescu et al. (2007), an extension of the study of Castañeda and Willis (1995), for thermal
 189 conductivity C_{cw} of a system of matrix and spheroidal inclusions are considered. A spheroidal
 190 distribution of the inclusions was supposed (Fig. 5b).

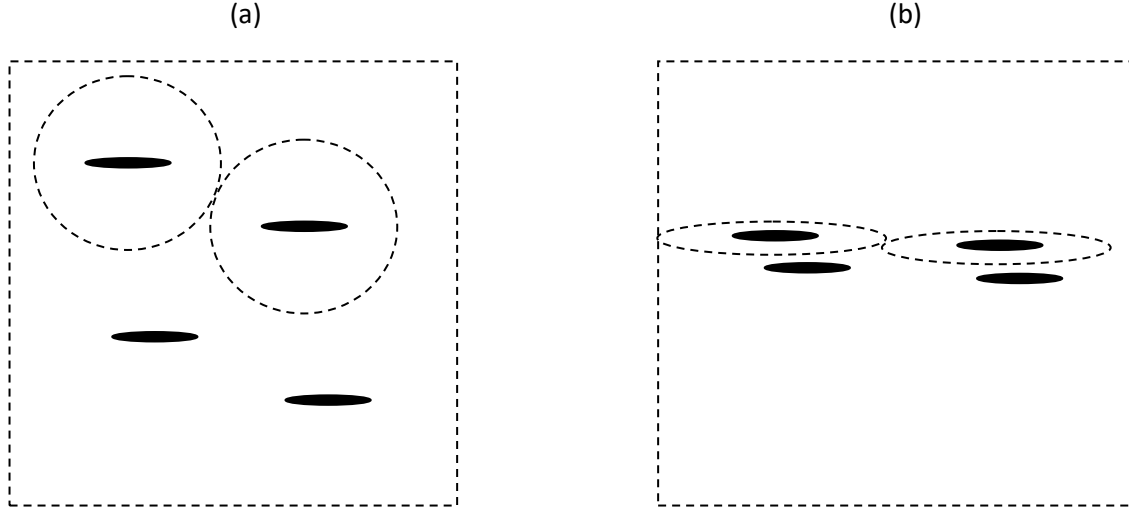
$$C_{cw}^N = C_m + f_I T_I^N \left(1 - f_I T_I^N \frac{1 - \frac{\pi}{2} X_d}{C_m} \right)^{-1} \quad (17)$$

$$C_{cw}^T = C_m + f_I T_I^T \left(1 - f_I T_I^T \frac{\frac{\pi}{4} X_d}{C_m} \right)^{-1}$$

191 with

$$T_I^N = \left(\frac{1}{C_I - C_m} + \frac{1 - \frac{\pi}{2} X}{C_m} \right)^{-1} ; T_I^T = \left(\frac{1}{C_I - C_m} + \frac{\frac{\pi}{4} X}{C_m} \right)^{-1} \quad (18)$$

192 where C_m and C_I are the conductivity of the matrix and of the inclusions respectively, f_I is the
 193 volume fraction of the inclusions, X_d is the aspect ratio of the distribution which equal to the
 194 aspect ratio of the MRP (Fig. 6b) (Castañeda and Willis, 1995). A parameter $X_d = 1$
 195 corresponds to a spherical distribution (Fig. 5a) and a parameter $X_d \rightarrow 0$ corresponds to a
 196 aligned distribution.



197

198 *Figure 5: Spatial distribution of cracks: spherical distribution (a) and aligned distribution (b).*

199 Applying eq. (17) for the case of inclusions are non-conducting cracks: $C_I = C_c = 0$ and $C_m =$

200 C_s :

$$C_{wc}^N = C_s - \frac{8C_s}{3}\epsilon \left(1 + \frac{8}{3}\epsilon \left(1 - \frac{\pi}{2}X_d\right)\right)^{-1} \quad (19)$$

$$C_{wc}^T = C_s$$

201 For the case of random orientation distribution of the crack:

$$C_{cw} = \frac{C_{cw}^N + 2C_{cw}^T}{3} = C_s - \frac{8C_s}{9}\epsilon \left(1 + \frac{8}{3}\epsilon \left(1 - \frac{\pi}{2}X_d\right)\right)^{-1} \quad (20)$$

202 Note that, for the particular case of aligned distribution of the cracks (the cracks lay closely in

203 the horizontal direction) $X_d \rightarrow 0$, (19) and (20) tend to (15) and (16):

$$\lim_{X_d \rightarrow 0} C_{wc}^N = C_s \left(1 - \frac{8}{3}\epsilon \left(1 + \frac{8}{3}\epsilon\right)^{-1}\right) = C_s \left(1 + \frac{8}{3}\epsilon\right)^{-1} \quad (21)$$

204 Analytical formulations (19) and (20) appear to be powerful to evaluate effective properties of

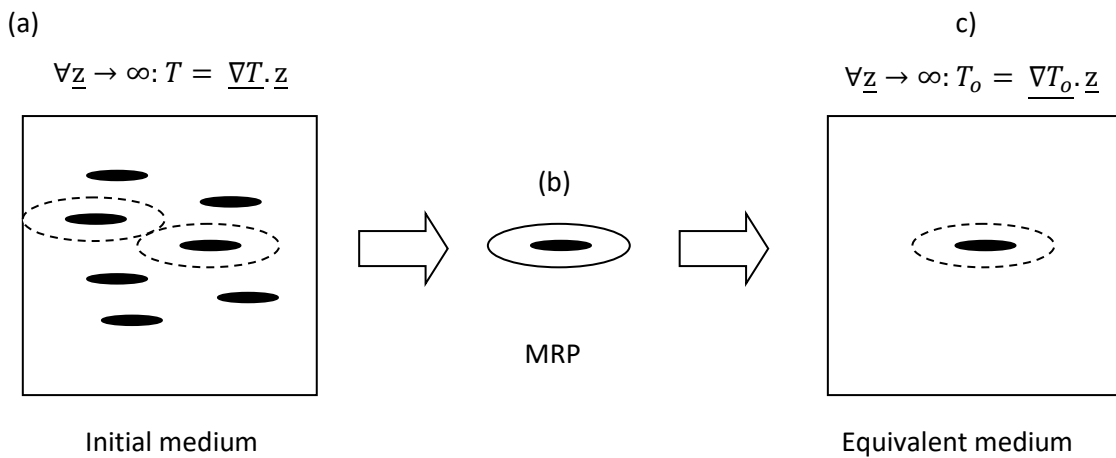
205 fractured materials. However they are limited to non-conducting penny-shape cracks. In the

206 next section, a numerical pattern-based approach will be proposed to deal with both the

207 spatial distribution and the conductivity of the cracks.

208 **3.2. Numerical pattern-based method**

209 PBM is developed to simulate heat flow and effective thermal conductivity of micro-cracked
 210 media. This method considers a MRP that, as described by Bornert et al. (1996), is a sub-
 211 domain containing a single crack that represents the microstructure of the whole domain (see
 212 Fig. 6b). In the numerical simulation, an equivalent domain formed by the MRP surrounded
 213 by an infinite matrix solid is considered (Nguyen and Dormieux, 2014) (Fig. 6c). The
 214 temperature boundary condition applied on the equivalent domain is: $\forall \underline{z} \rightarrow \infty: T_o = \underline{\nabla T}_o \cdot \underline{z}$. To
 215 account for the interaction between the cracks, the equivalent temperature gradient $\underline{\nabla T}_o$ is
 216 chosen to ensure that the average temperature of the MRP is equal to the macroscopic
 217 temperature gradient applied on the initial medium that was noted by $\underline{\nabla T}$ (see Mori and
 218 Tanaka, 1973). The numerical simulation of the equivalent problem is similar to the problem
 219 presented in the section 2. By using the FEM code Cast3M, the temperature and the heat
 220 flux field in the whole equivalent domain can be obtained.



221

222 *Figure 6: MRP (b) of a fractured medium (a) and its equivalent medium for numerical*
 223 *simulation (c).*

224 The macroscopic heat flux is calculated by taking the average over the MRP inside the
 225 equivalent domain.

$$\underline{F} = \frac{1}{V_{MRP}} \int_{MRP} \underline{f} dV \quad (22)$$

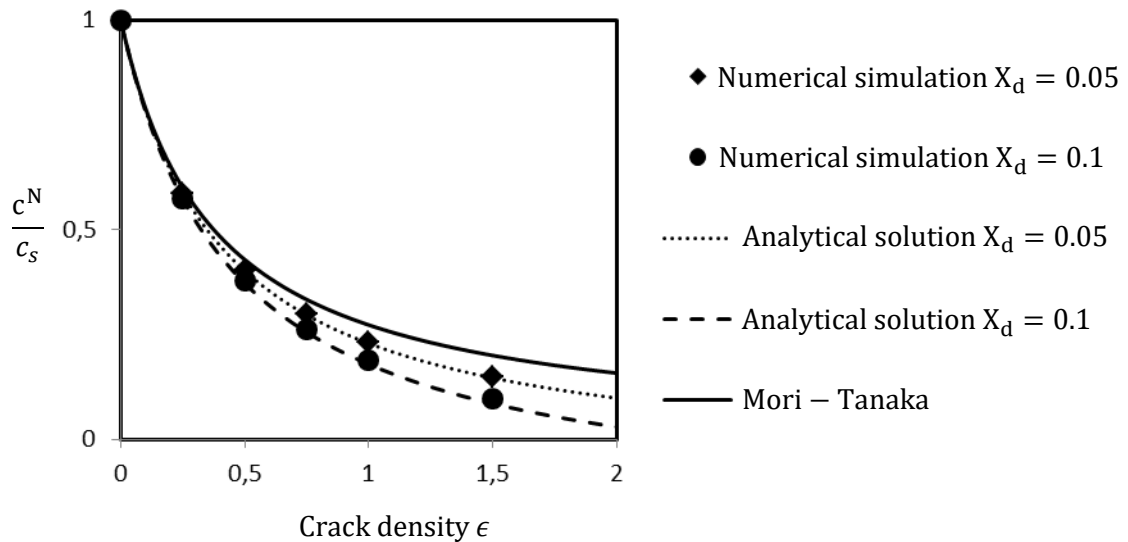
226 Then the effective conductivity is calculated, for the case of parallel cracks, by:

$$C^N = \frac{F_3}{\nabla T_3}; C^T = C_s \quad (23)$$

227 and for random orientation distribution of cracks by:

$$C = \frac{C^N + 2C^T}{3} \quad (24)$$

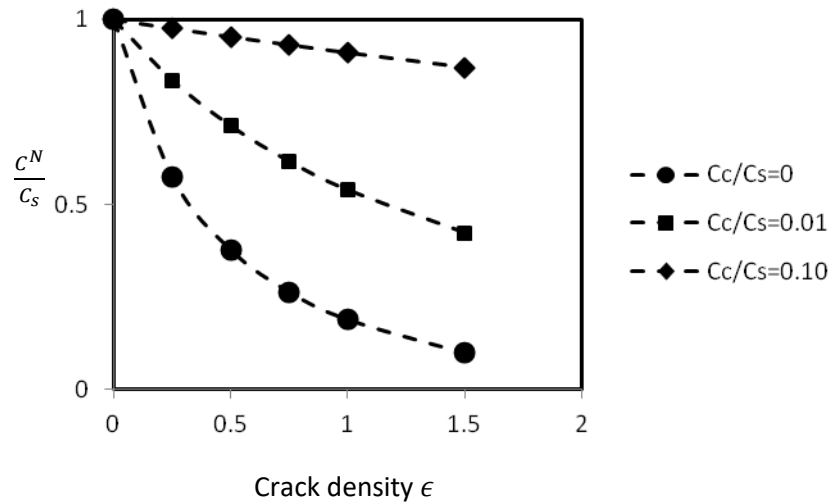
228 Fig. 7 shows a comparison between the numerical simulation obtained by current method
 229 and the analytical solutions derived in previous section, for the case of parallel non-
 230 conducting cracks. A perfect fit between the numerical approach and the analytical approach
 231 (eq. (19)) can be observed. It is to note that both approaches consider the spatial distribution
 232 of the cracks. Two distribution was considered: $X_d = 0.1$ and $X_d = 0.05$. The numerical
 233 results also show that, as presented in eq. (21), when X_d tends to zero the conductivity tends
 234 to that obtained by the Mori-Tanaka method (eq. (15)).



235

236 *Figure 7: Comparison between the numerical PBM and the analytical homogenization-based*
 237 *approach.*

238 Note that, differently from the analytical solutions, the numerical method also allows the
 239 simulation of the effective conductivity media containing conducting cracks. Fig. 8 shows the
 240 effect of the crack conductivity on the overall conductivity of the medium. The simulation
 241 suggests that, for $C_c/C_s \geq 0.1$, the effect of cracks on the overall conductivity of the fractured
 242 media is weak.



243

244 *Figure 8: Effect of crack conductivity and crack density on overall conductivity of fractured*
 245 *media: numerical simulations.*

246 **4. Conclusions**

247 Firstly, heat flow across a single crack is analyzed by both analytical and numerical methods.
 248 A closed-form solution is derived for the temperature jump across a single non-conducting
 249 crack under homogeneous gradient far-field boundary condition. This analytical formulation is
 250 then validated by the FEM simulation. The effect of crack conductivity on the temperature
 251 discontinuity is also analyzed by the numerical method. It is shown that for crack of high
 252 conductivity (for example water saturated crack), the temperature jump across the crack can
 253 be negligible and the crack affects weakly the heat flow through the whole medium.

254 Secondly, the basic result of heat flow across a single crack is extended for the case of
 255 multiple cracks. Homogenization-based analytical approaches and PBM are employed to

256 simulate effective thermal conductivity of fractured materials. Both isotropic and transversely
257 isotropic (parallel cracks) cases are considered. The spatial distribution of the cracks is also
258 taken into account in the analytical and numerical methods. In the particular case of non-
259 conducting crack, the numerical and analytical methods fit perfectly together. When the
260 distribution of the crack is aligned, both approaches tend to the analytical solution developed
261 based on the Mori-Tanaka scheme.

262 The numerical PBM allows also the simulation of the effect of the crack conductivity on the
263 overall conductivity of the fractured media. It is demonstrated that, for cracks with
264 conductivity equal to of about 10% of the conductivity of the surrounding solid matrix (for
265 example water saturated rocks), the effect of the cracks system on the overall conductivity of
266 the fractured media can be negligible.

267 **References**

268 Tang, A. M., & Cui, Y. J. (2009). Modelling the thermo-mechanical volume change behaviour
269 of compacted expansive clays. *arXiv preprint arXiv:0904.3614*.

270 Tang, A. M., Cui, Y. J., & Le, T. T. (2008). A study on the thermal conductivity of compacted
271 bentonites. *Applied Clay Science*, 41(3), 181-189.

272 Bentejac, F., & Hourdequin, N. (2005). TOUTATIS: An Application of the Cast3m Finite
273 Element Code for PCI Three-Dimensional Modelling. In *Pellet-Clad Interaction in Water*
274 *Reactor Fuels*.

275 Bornert, M. (1996). A generalized pattern-based self-consistent scheme. *Computational*
276 *Materials Science*, 5(1), 17-31.

277 Bornert, M., Stolz, C., & Zaoui, A. (1996). Morphologically representative pattern-based
278 bounding in elasticity. *Journal of the Mechanics and Physics of Solids*, 44(3), 307-331.

279 Budiansky, B., & O'connell, R. J. (1976). Elastic moduli of a cracked solid. *International*
280 *Journal of Solids and Structures*, 12(2), 81-97.

281 Camacho, G. T., & Ortiz, M. (1996). Computational modelling of impact damage in brittle
282 materials. *International Journal of Solids and Structures*, 33(20), 2899-2938.

283 Castañeda, P. P., & Willis, J. R. (1995). The effect of spatial distribution on the effective
284 behavior of composite materials and cracked media. *Journal of the Mechanics and Physics
285 of Solids*, 43(12), 1919-1951.

286 Clauser, C., & Huenges, E. (1995). Thermal conductivity of rocks and minerals. *Rock physics
287 & phase relations: A handbook of physical constants*, 105-126.

288 Cui, Y. J., Tang, A. M., Qian, L. X., Ye, W. M., & Chen, B. (2011). Thermal-mechanical
289 behavior of compacted GMZ Bentonite. *Soils and foundations*, 51(6), 1065-1074.

290 Dormieux, L., Kondo, D., & Ulm, F. J. (2006). *Microporomechanics*. John Wiley & Sons.

291 Eshelby, J. (1957). The determination of the elastic field of an ellipsoidal inclusion and
292 related problems. *Proc. R. Soc. London, A* 241, 376–396.

293 Giraud, A., Gruescu, C., Do, D. P., Homand, F., & Kondo, D. (2007). Effective thermal
294 conductivity of transversely isotropic media with arbitrary oriented ellipsoidal
295 inhomogeneities. *International Journal of Solids and Structures*, 44(9), 2627-2647.

296 Gruescu, C., Giraud, A., Homand, F., Kondo, D., & Do, D. P. (2007). Effective thermal
297 conductivity of partially saturated porous rocks. *International Journal of Solids and
298 Structures*, 44(3), 811-833.

299 Mori, T., & Tanaka, K. (1973). Average stress in matrix and average elastic energy of
300 materials with misfitting inclusions. *Acta metallurgica*, 21(5), 571-574.

301 Nguyen, ST (2014a). Micromechanical approach for electrical resistivity and conductivity of
302 sandstone. *Journal of Applied Geophysics*, 111, 135-140.

303 Nguyen, ST (2014b) Generalized Kelvin model for micro-cracked viscoelastic
304 materials. *Engineering Fracture Mechanics*, 127, 226-234.

305 Nguyen, S. T., & Dormieux, L. (2014). Propagation of micro-cracks in viscoelastic materials:
306 Analytical and numerical methods. *International Journal of Damage Mechanics*,
307 1056789514539715.

308 Nguyen, ST, Dormieux, L, Le Pape, Y & Sanahuja, J (2011) A Burger model for the effective
309 behavior of a microcracked viscoelastic solid. *International Journal of Damage Mechanics*,
310 20(8), 1116-1129.

311 Nguyen, ST, Vu, MH, & Vu, MN (2015a). Extended analytical approach for electrical
312 anisotropy of geomaterials. *Journal of Applied Geophysics*, 123, 211-217.

313 Nguyen, S. T., Vu, M. H., & Vu, M. N. (2015b). Equivalent porous medium for modeling of the
314 elastic and the sonic properties of sandstones. *Journal of Applied Geophysics*, 120, 1-6.

315 Nguyen, TN, Nguyen, ST, Vu, MH, & Vu, MN (2015c). Effective viscoelastic properties of
316 micro-cracked heterogeneous materials. *International Journal of Damage Mechanics*,
317 1056789515605557.

318 Pouya, A., Vu, M. N., Ghabezloo, S., & Bendjeddou, Z. (2013). Effective permeability of
319 cracked unsaturated porous materials. *International Journal of Solids and Structures*, 50(20),
320 3297-3307.

321 Stolz, C., & Zaoui, A. (1991). Analyse morphologique et approches variationnelles du
322 comportement d'un milieu élastique hétérogène. *Comptes rendus de l'Académie des*
323 *sciences. Série 2, Mécanique, Physique, Chimie, Sciences de l'univers, Sciences de la*
324 *Terre*, 312(3), 143-150.

325 Vu, M. N., Nguyen, S. T., Vu, M. H., Tang, A. M., To, V. T. (2015). Heat conduction and
326 thermal conductivity of 3D cracked media. *International Journal of Heat and Mass Transfer*
327 89, 1119-1126.

328 Zimmerman, R. W. (1989). Thermal conductivity of fluid-saturated rocks. *Journal of*
329 *Petroleum Science and Engineering*, 3(3), 219-227.

330